

# Spin Hamiltonian, Order Out of a Coulomb Phase and Pseudo-Criticality in the Highly Frustrated Pyrochlore Heisenberg Antiferromagnet $\text{FeF}_3$

Azam Sadeghi,<sup>1</sup> Mojtaba Alaei,<sup>1,\*</sup> Farhad Shahbazi,<sup>1,†</sup> and Michel J. P. Gingras<sup>2,3,4,‡</sup>

<sup>1</sup>*Department of Physics, Isfahan University of Technology, Isfahan 84156-83111, Iran*

<sup>2</sup>*Department of Physics and Astronomy, University of Waterloo, Waterloo, ON, N2L 3G1, Canada*

<sup>3</sup>*Perimeter Institute for Theoretical Physics, 31 Caroline North, Waterloo, ON, N2L 2Y5, Canada*

<sup>4</sup>*Canadian Institute for Advanced Research, 180 Dundas Street West, Suite 1400, Toronto, ON, M5G 1Z8, Canada*

(Dated: April 4, 2024)

$\text{FeF}_3$ , with its half-filled  $\text{Fe}^{3+}$  3d orbital, hence zero orbital angular momentum and  $S = 5/2$ , is often put forward as a prototypical highly-frustrated classical Heisenberg pyrochlore antiferromagnet. By employing *ab initio* density functional theory (DFT), we obtain an effective spin Hamiltonian for this material. This Hamiltonian contains nearest-neighbor antiferromagnetic Heisenberg, bi-quadratic and Dzyaloshinskii-Moriya interactions as dominant terms and we use Monte Carlo simulations to investigate the nonzero temperature properties of this minimal model. We find that upon decreasing temperature, the system passes through a Coulomb phase, composed of short-range correlated coplanar states, before transforming into an “all-in/all-out” (AIAO) state via a very weakly first order transition at a critical temperature  $T_c \approx 22$  K, in good agreement with the experimental value for a reasonable set of Coulomb interaction  $U$  and Hund’s coupling  $J_H$  describing the material. Despite the transition being first order, the AIAO order parameter evolves below  $T_c$  with a power-law behavior characterized by a pseudo “critical exponent”  $\beta \approx 0.18$  in accord with experiment. We comment on the origin of this unusual  $\beta$  value.

PACS numbers: 71.15.Mb, 75.40.Mg, 75.10.Hk, 75.30.Gw

Systems with magnetic moments on the vertices of two- and three-dimensional networks of corner-shared triangles or tetrahedra and with predominant effective antiferromagnetic nearest-neighbor (n.n.) interactions have tenuous tendency towards conventional long-range magnetic order [1, 2]. Consequently, the exotic low-temperature properties of materials with such an architecture are ultimately dictated by the mutual competition of perturbations beyond n.n. interactions [2].

One theoretically expects such highly-frustrated magnets to ubiquitously display a *Coulomb phase* (CP) [3]. This is an emergent state with local constraints described by a divergence-free “spin field” and whose defects, where the constraints are violated, behave as effective charges with Coulombic interactions. The CP and its underlying gauge theory description provides an elegant setting to study the effect of various perturbations [4] as well as thermal and quantum fluctuations [5]. A telltale experimental signature of a CP are bow-tie (“pinch points”) singularities in the energy-integrated neutron scattering intensity pattern [3, 11].

There is good evidence that the classical spin liquid state of spin ice materials with discrete Ising spins may be described by a CP [3, 7–9]. Unfortunately, there are few, if any, materials with continuous symmetry spins that display a CP, as may be signalled by pinch points [11]. For example, in  $\text{Y}_2\text{Mo}_2\text{O}_7$ , complex orbital effects

[10, 11] and spin glass behavior [12, 13] irradiate the CP. In the  $\text{ZnCr}_2\text{O}_4$  spinel, pinch points are not observed [14], likely because perturbations beyond n.n. interactions and spin-lattice coupling eliminate them already at high temperature in the paramagnetic state [4]. In this letter we propose that  $\text{FeF}_3$ , with magnetic  $\text{Fe}^{3+}$  ions on a pyrochlore network of corner-sharing tetrahedra, may be a strong contender for a CP with Heisenberg spins.

With  $\text{Fe}^{3+}$  being a 3d S-state (spin-only)  $S = 5/2$  ion, single-ion anisotropy and anisotropic spin-spin interactions should be small in  $\text{FeF}_3$ , making it a good candidate material with predominant n.n. Heisenberg exchange. Neutron scattering and Mössbauer experiments find long-range magnetic order below  $T_c \approx 20_{-5}^{+2}$  K [2, 16–19]. Yet, the static magnetic susceptibility shows a deviation from the Curie-Weiss law even at 300 K, implying the existence of strong antiferromagnetic exchange and short-range correlations extending up to temperatures much higher than  $T_c$  [2] and thus a very high degree of frustration [2, 20]. The ordered phase is an “all-in/all-out” (AIAO) state [2] in which the  $\text{Fe}^{3+}$  magnetic moments point from the corners to the centers (or vice versa) of each tetrahedron (see Fig. 1a). Notably, neutron diffraction experiments find a power-law growth of the AIAO order parameter characterized by a “critical exponent”  $\beta \sim 0.18$  [19]. This value differs significantly from standard order-parameter exponents  $\beta \sim 1/3$  for three-dimensional systems, which prompted the suggestion of an underlying “new” universality class [19]. There appears to have been no attempt to determine a realistic spin Hamiltonian  $\mathcal{H}$  for  $\text{FeF}_3$ . In this paper, we employ density-functional theory (DFT) to flesh out such  $\mathcal{H}$  and use it to study the development of correlations

\*Electronic address: m.alaei@cc.iut.ac.ir

†Electronic address: shahbazi@cc.iut.ac.ir

‡Electronic address: gingras@uwaterloo.ca

upon approaching  $T_c$  and to explore the associated critical properties. By computing the energy of various spin configurations and performing Monte Carlo simulations, we expose a highly entropic coplanar (Coulombic) state above  $T_c$  and its demise at  $T \leq T_c$  against an energetically selected AIAO state along with replicating the unusual  $\beta \sim 0.18$  exponent.

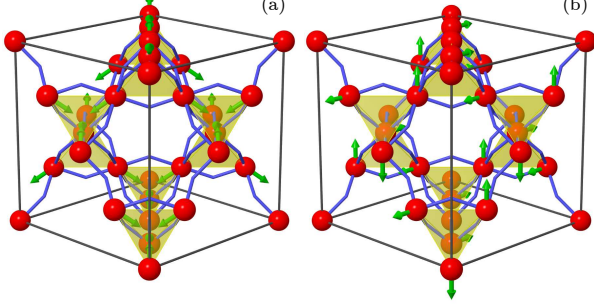


FIG. 1: (Color online): The structure of  $\text{FeF}_3$ . Red (dark grey) spheres denote the  $\text{Fe}^{3+}$  ions with their spin indicated by a green arrow. The  $\text{F}^-$  ions (not shown) are located at the (shown) bents where bonds merge. (a) The AIAO state. (b) A coplanar spin configuration (for clarity, a long-range coplanar state is shown).

*Spin Hamiltonian and DFT calculations* – The classical spin Hamiltonian for  $\text{FeF}_3$  is given by

$$\mathcal{H} = \mathcal{H}_H + \mathcal{H}_{\text{b.q.}} + \mathcal{H}_r + \mathcal{H}_{\text{DM}} + \mathcal{H}_{\text{s.i.}}. \quad (1)$$

$\mathcal{H}_H = \sum_{i>j} J_{ij} \mathbf{S}_i \cdot \mathbf{S}_j$  denotes the isotropic Heisenberg term.  $\mathbf{S}_i$  and  $\mathbf{S}_j$  are classical unit vectors representing the orientation of the magnetic moments at sites  $i$  and  $j$ , respectively. We consider a distance-dependent exchange  $J_{ij}$  between  $\mathbf{S}_i$  and  $\mathbf{S}_j$ , with first ( $J_1$ ), second ( $J_2$ ) and two distinct third ( $J_{3a}$  and  $J_{3b}$ ) n.n. [21].  $\mathcal{H}_{\text{b.q.}} = \sum_{i>j} B_{ij} (\mathbf{S}_i \cdot \mathbf{S}_j)^2$  is the bi-quadratic interaction with n.n. coupling  $B_1$ .  $\mathcal{H}_r = \sum_{ijkl} K[(\mathbf{S}_i \cdot \mathbf{S}_j)(\mathbf{S}_k \cdot \mathbf{S}_l) + (\mathbf{S}_j \cdot \mathbf{S}_k)(\mathbf{S}_l \cdot \mathbf{S}_i) - (\mathbf{S}_i \cdot \mathbf{S}_k)(\mathbf{S}_j \cdot \mathbf{S}_l)]$  is the ring-exchange interaction. The last two (anisotropic interaction) terms, originating from spin-orbit coupling (SOC), are the Dzyaloshinskii-Moriya (DM) interaction,  $\mathcal{H}_{\text{DM}} = D \sum_{\langle i,j \rangle} \hat{\mathbf{D}}_{ij} \cdot (\mathbf{S}_i \times \mathbf{S}_j)$ , and single-ion anisotropy  $\mathcal{H}_{\text{s.i.}} = \Delta \sum_i (\mathbf{S}_i \cdot \hat{\mathbf{d}}_i)^2$ .  $\hat{\mathbf{D}}_{ij}$  are the DM (unit) vectors determined according to the Moriya rules [7, 23]. The unit vector  $\hat{\mathbf{d}}_i$  denotes the single-ion easy-axis along the local cubic [111] direction at site  $i$ .

We next use DFT to study the properties of  $\text{FeF}_3$ . For all computations, the experimental data for the conventional cubic unit cell lattice parameter (10.325 Å) and position of the ions were used [16]. The DFT calculations were carried out with the full-potential linearized augmented plane wave (FLAPW) method, employing the Fleur code [31]. We used the local density approximation (LDA) to account for the electron exchange-correlation. Electron-electron interactions due to the on-site electron repulsion  $U$  are taken into account using the LDA+ $U$

method. The effective on-site Coulomb interaction,  $U_{\text{eff}}$ , is defined as  $U_{\text{eff}} = U - J_H$ , where  $U$  is the bare Coulomb repulsion and  $J_H$  is the on-site ferromagnetic Hund's exchange, which we set to 1.0 eV, a typical value in such DFT calculations. Using a linear response approach [32], we obtain  $U_{\text{eff}} \approx 2.8$  eV from the Quantum-Espresso code [33]. The influence of  $U_{\text{eff}}$  on various properties is discussed in the Supplementary Material (S.M.) [23]. The minimum energy states possess a global continuous  $O(3)$  degeneracy within LDA+ $U$ . However, incorporating the effect of SOC within LDA+ $U$ +SOC leads to an AIAO configuration with spins along  $\langle 111 \rangle$  as minimum energy state. We find  $\text{FeF}_3$  to be an insulator with a 1.04 eV band gap within LDA+SOC. The band gap rises to 2.49 eV in LDA+ $U$ +SOC with  $U_{\text{eff}} = 2.8$  eV.

We next determine the coupling constants of  $\mathcal{H}$  using spin-polarized DFT calculations. For the first three (isotropic) terms of Eq. (1), we use LDA+ $U$  to compute the total energy difference between various magnetic configurations [23]. We assume that  $J_{3b}$  [21] as well as farther Heisenberg exchanges ( $J_m, m \geq 4$ ), and bi-quadratic terms further than first n.n. ( $B_m, m \geq 2$ ) are negligible. By matching the energy differences for spin-polarized electronic states with that of  $\mathcal{H}$ , we determine  $J_1, J_2, J_{3a}$  and  $B_1$  [23]. To compute the anisotropic DM ( $D$ ) and single-ion ( $\Delta$ ) couplings arising from SOC, we use the LDA+ $U$ +SOC framework. We consider non-collinear spin-polarized configurations, keeping the isotropic terms of  $\mathcal{H}$  unchanged [23]. The largest couplings within LDA+ $U$ +SOC are (all in meV):

$$J_1 = 32.7, J_2 = 0.6, J_{3a} = 0.5, B_1 = 1.0, D = 0.6. \quad (2)$$

The ring-exchange  $K$  and the single-ion coupling  $\Delta$  are found to be smaller than 0.1 meV [23], so we henceforth ignore them. The Curie-Weiss temperature,  $\theta_{\text{CW}}$ , can thus be estimated by  $\theta_{\text{CW}} \sim qJ_1/3 \sim 760$  K, where  $q = 6$  is the number of n.n. With  $\theta_{\text{CW}}/T_c \sim 38$ , we thus confirm  $\text{FeF}_3$  to be a highly-frustrated antiferromagnet [2, 20].

*Ground states and Monte Carlo simulations* – Following Refs. [34, 35], we find that mean-field theory predicts AIAO order for  $\mathcal{H}$  with the above  $\{J_1, J_2, J_{3a}, D\}$  values and  $B_1 \equiv 0$ . This is confirmed by MC simulations when including  $B_1 = 1.0$  meV since ( $B_1 > 0, D = 0$ ) stabilizes an  $O(3)$  symmetric AIAO state (see discussion below). In the rest of the paper, we focus on the *generic* aspects of the collective behavior of the system (such as exponent  $\beta \sim 0.18$ ). While specific details ( $T_c$ , and the Fe and F magnetic moments) depend on the value of the ( $U, J_H$ ) parameters [23], we expect the overall collective properties to survive small adjustments of these parameters [23]. Therefore, to explore those generic facets, we consider a minimal model Hamiltonian,  $\mathcal{H}_{\text{min}}$ , with  $\mathcal{H}_{\text{min}} \equiv \mathcal{H}(J_1, B_1, D, J_2 = J_{3a} = 0)$  with the ( $J_1, B_1, D$ ) values of Eq. (2).

The ground state of  $\mathcal{H}_{\text{min}}$  with ( $J_1 > 0, B_1 = D = 0$ ), is highly degenerate on the pyrochlore lattice [1, 35–37]. The ground state manifold consists of spin configurations with vanishing total spin on each tetrahedron, with two

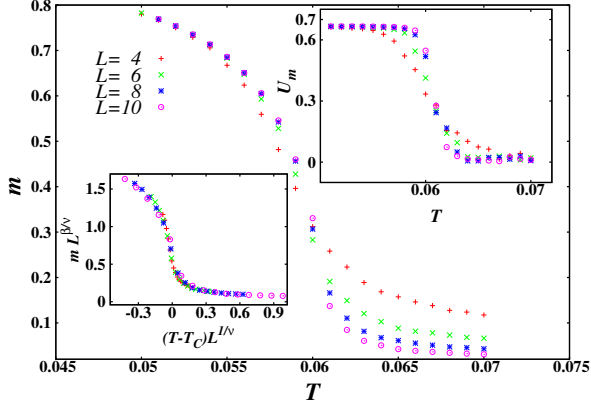


FIG. 2: (Color online) main panel: variation of the AIAO order parameter ( $m$ ) versus temperature (in units of  $J_1$ ), for lattices of linear size  $L = 4, 6, 8, 10$ . Top inset: Fourth order Binder cumulant of  $m$  versus temperature,  $T$  (in units of  $J_1$ ), for the same lattice sizes. Left inset: Finite size scaling of  $m(t, L)$  with  $\beta = 0.18(2)$  and  $\nu = 0.60(2)$ .

continuous degrees of freedom per tetrahedron [23, 35–37]. The minimum energy of  $\mathcal{H}_{\min}$  with  $(J_1 > 0, B_1 > 0, D = 0)$  has a globally  $O(3)$  degenerate non-coplanar AIAO spin configuration with an angle  $109.47^\circ$  between each n.n. pair of spins [23]. Including  $D > 0$  fixes the spin directions within such a configuration to one of two discrete AIAO states with spins along the cubic  $\langle 111 \rangle$  directions [23]. With  $B_1 = 0$ , direct DM interactions ( $D > 0$ ) also dictates an AIAO state [7]. The ground state energy per spin [23] for the coplanar and AIAO state is, respectively,  $\epsilon_{\text{coplanar}} = -J_1 + B_1 - \sqrt{2}D$  and  $\epsilon_{\text{AIAO}} = -J_1 + B_1/3 - 2\sqrt{2}D$ , showing that the ground state is AIAO for all  $B_1 > 0$  and  $D > 0$  values.

With  $(J_1 > 0, B_1 > 0, D = 0)$ ,  $\mathcal{H}_{\min}$  displays for a tetrahedron three saddle points in its energy landscape which correspond to coplanar states [23]. In these states, two out of four spins are antiparallel along a given axis and perpendicular to the other axis along which the two remaining spins are themselves aligned mutually antiparallel. The addition of  $D > 0$  restricts the orientation of the “coplanes” to be along the  $xz$ ,  $xy$  or  $yz$  planes of the cubic unit cell, depending on which pairs of spins are chosen to be collinear [23]. There is an exponentially large number of such coplanar states which provide an entropy buffer above the critical temperature where the system orders into AIAO. One such coplanar spin arrangement, within the  $xz$  plane, is depicted in Fig. 1b.

We next perform Monte Carlo simulations to gain some insight into the finite temperature properties of  $\mathcal{H}_{\min}$ . We use standard single-spin Metropolis algorithm on lattices consisting of  $N = 4 \times L^3$  spins, where  $L$  is the linear dimension of the rhombohedral simulation cell. To ensure thermal equilibrium,  $10^6$  Monte Carlo steps (MCS) per spin were used for each temperature and  $10^6$  MCS for the data collection. To reduce the correlation between measurements, 10 to 20 MC sweeps were discarded between

successive data collection. To ascertain that our results are fully thermally equilibrated and are not caused by a two-phase coexistence, we started the simulation runs from different initial states, i.e. totally disordered, AIAO ordered and coplanar states and checked that all final results remain the same.

Quantities of particular interest are the AIAO order parameter  $m \equiv \Sigma_{i,a} \mathbf{S}_i^a \cdot \hat{\mathbf{d}}^a / N$  ( $\hat{\mathbf{d}}^a$  is the local cubic  $\langle 111 \rangle$  direction for sublattice  $a$ ) and the Binder fourth order cumulant for both  $m$  and energy  $E$ , defined respectively as  $U_m(T) \equiv 1 - \frac{1}{3} \frac{\langle m^4 \rangle}{\langle m^2 \rangle^2}$  and  $U_E(T) \equiv 1 - \frac{1}{3} \frac{\langle E^4 \rangle}{\langle E^2 \rangle^2}$ .  $U_m$  vanishes in the paramagnetic phase, with a Gaussian probability distribution for  $m$ , while  $U_m$  approaches  $2/3$  in the ordered phase [9, 38, 39].  $U_E$  tends asymptotically to  $2/3$  in both the ordered and paramagnetic phase while reaching a minimum,  $U_E^{\min}$ , near the transition [23].

The temperature dependence of  $m$  and  $U_m$  is shown in the main panel and top inset of Fig. (2). Both plots indicate a narrow critical region around  $T \approx 0.06$ . The left inset in Fig. 2 shows the finite-size scaling of  $m$  for different  $L$  according to the finite-size scaling behavior  $m = L^{-\beta/\nu} \mathcal{M}(tL^{1/\nu})$ . Here  $t \equiv (T_c - T)/T_c$  is the reduced temperature,  $\beta$  is the order parameter exponent,  $\nu$  is the correlation length exponent and  $\mathcal{M}$  is the scaling function [9]. This analysis yields  $T_c/J_1 = 0.0601(2)$ ,  $\beta = 0.18(2)$  and  $\nu = 0.60(2)$ . With  $J_1 = 32.7$  meV = 379.47 K, we get  $T_c \approx 22$  K, in good agreement with the experimental value [2, 16, 17, 19]. Perhaps most noteworthy, the Monte Carlo exponent  $\beta \approx 0.18$  value corresponds to that found in experiment [19]. While these scaling arguments naively suggest that the transition is second order, it is instructive to consider the  $L$  dependence of  $U_E^{\min}$  which, for a first order transition, is given by [9],  $U_E^{\min}(L) = U^* + AL^{-d} + \mathcal{O}(L^{-2d})$ , with  $U^* < 2/3$ . Here  $d = 3$  is the space dimension and  $A$  is a constant. The precise linear fit of  $U_E^{\min}(L)$  versus  $L^{-3}$ , with  $U^* = 0.666664(1)$ , hence very close to  $2/3$ , that we find (see Fig. 13 in the S.M. [23]) suggests that the transition might actually be very weakly first order.

To shed further light on the nature of the transition, we compute the probability distribution function of the order parameter per tetrahedron,  $P(m_n)$ , with  $m_n \equiv \Sigma_{a=1}^4 \mathbf{S}^a \cdot \hat{\mathbf{d}}^a$ . We also compute the probability distribution function of two distinct four-spin correlations within each tetrahedron,  $P(R)$  and  $P(\tilde{R})$ , with

$$R \equiv (\mathbf{S}_1 \cdot \mathbf{S}_2)(\mathbf{S}_3 \cdot \mathbf{S}_4) + (\mathbf{S}_1 \cdot \mathbf{S}_3)(\mathbf{S}_2 \cdot \mathbf{S}_4) + (\mathbf{S}_1 \cdot \mathbf{S}_4)(\mathbf{S}_2 \cdot \mathbf{S}_3),$$

$$\tilde{R} \equiv |(\mathbf{S}_1 \cdot \mathbf{S}_2)(\mathbf{S}_3 \cdot \mathbf{S}_4) - (\mathbf{S}_1 \cdot \mathbf{S}_3)(\mathbf{S}_2 \cdot \mathbf{S}_4) + (\mathbf{S}_1 \cdot \mathbf{S}_4)(\mathbf{S}_2 \cdot \mathbf{S}_3)|.$$

Figures 3a, 3b and 3c show  $P(m_n)$ ,  $P(R)$  and  $P(\tilde{R})$  versus  $T$  for  $L = 10$ .  $P(m_n)$  is a Gaussian centered at  $m_n = 0$  for  $T \gg T_c$ . As  $T$  decreases,  $P(m_n)$  deviates from a Gaussian near  $T_c$ , developing *four* peaks with  $m_n \neq 0$  for  $T \lesssim T_c$ . Well below the transition, only two peaks at  $|m_n| \approx 4$  remain, corresponding to almost perfect AIAO order. The peculiar temperature evolution of  $P(m_n)$  suggests that another state coexists or competes with the AIAO state near  $T_c$ . The nature of this other state can be clarified by considering  $P(R)$  and



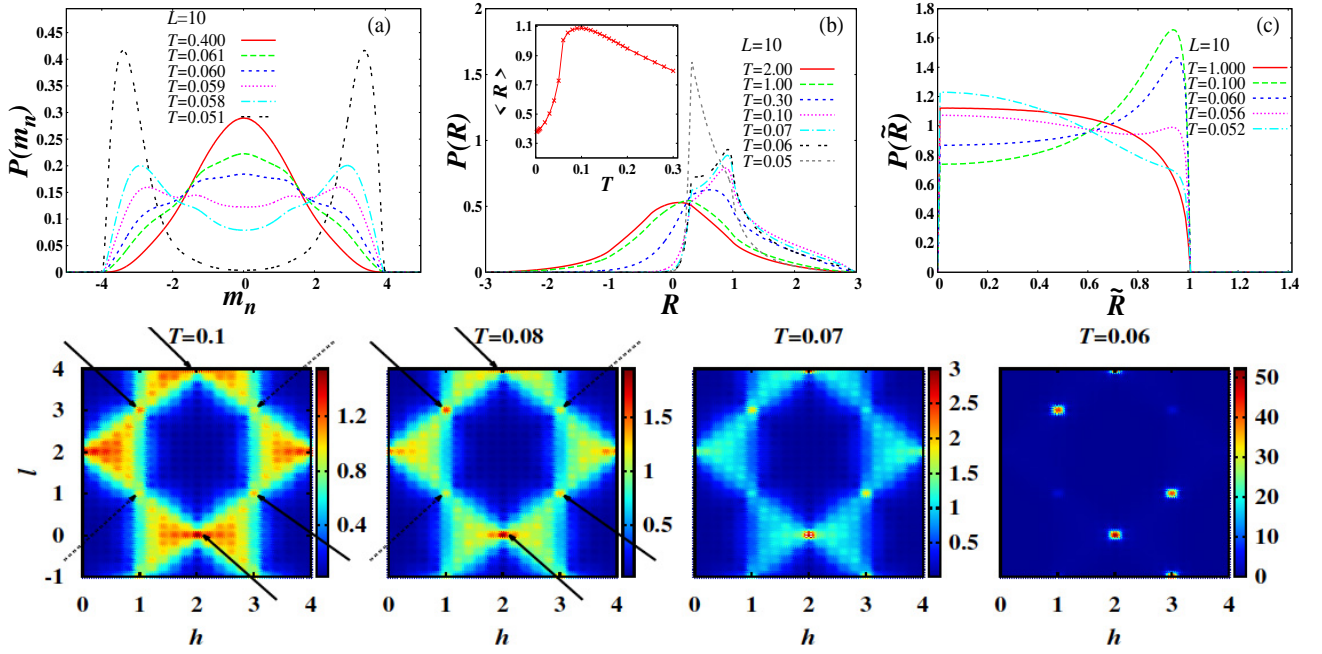


FIG. 3: (Color online) **Top row:** Probability distribution functions,  $P(m_n)$ ,  $P(R)$  and  $P(\tilde{R})$ , as a function of temperature  $T$  and for a lattice of linear size  $L = 10$ . The inset of panel (b) shows the  $T$  dependence of  $\langle R \rangle$ , which displays a sharp drop at  $T_c \approx 0.06$ , a further indication for the discontinuous nature of the transition. **Bottom row:** Temperature evolution of the neutron structure factor,  $S(\mathbf{q})$ , in the  $(hhl)$  plane as  $T$  approaches  $T_c$  from the paramagnetic phase. The arrows indicate the location of pinch points for the  $T = 0.1$  and  $T = 0.08$  panels (see text).

$P(\tilde{R})$  in Figs. 3b and 3c, respectively. Two peaks arise in  $P(R)$  at  $T \gtrsim T_c$ ; one at  $R \approx 1/3$  and another at  $R \approx 1$  (see panel 3b). The former corresponds to an AIAO spin configuration for which  $(\mathbf{S}_a \cdot \mathbf{S}_b) = -\frac{1}{3}$  at  $T \ll J_1$  for two n.n. spins. The peak at  $R = 1$  is consistent with coplanar states as deduced from Eq. (20). Considering  $P(\tilde{R})$  in Fig. 3c, one observes a peak at  $\tilde{R} \approx 1$  near  $T_c$ . One can easily show [23] that the two equations for  $R = 1/3$  and  $\tilde{R} = 1$  have *no common* solution for a zero net spin/moment on a tetrahedron. Therefore, an AIAO state does not produce the peak at  $\tilde{R} \approx 1$ , which must therefore originate from the competing state. One can show that Eqs. (20) for  $R = 1$  and  $\tilde{R} = 1$  admit three solutions [23], which are precisely the  $xy$ ,  $xz$  and  $yz$  coplanar states discussed above. The “competing state” at  $T \gtrsim T_c$  is therefore short-range coplanar, as illustrated further in the S.M. [23], is divergence-free in the “spin field” and should thus be viewed as a CP [3]. To expose further the CP nature of the state at  $T \gtrsim T_c$ , we compute the neutron structure factor  $S(\mathbf{q})$  (second row of Fig. 3) in the  $(hhl)$  scattering plane as a function of  $T$ . At  $T = 0.1$ , clear pinch points (marked by arrows) are visible. Some of these pinch points (solid arrows) turn into magnetic Bragg peaks ( $T \sim 0.06$ ) while others (dashed arrows) become mere weak diffuse spots (forbidden Bragg peaks [23]) upon going through the transition to AIAO order at  $T_c$  (see  $T = 0.08, T = 0.07$  and  $T = 0.06$  panels in bottom row of Fig. 3).

*Conclusion* – Using DFT, we determined the pre-

dominant couplings of the spin Hamiltonian of the  $\text{FeF}_3$  pyrochlore Heisenberg antiferromagnet. We find that bi-quadratic exchange and anisotropic direct Dzyaloshinskii-Moriya interactions conspire to select an all-in/all-out ground state. Monte Carlo simulations find a transition to that state at a critical temperature  $T_c \approx 22$  K, in good agreement with experiments. The transition is characterized by an order parameter pseudo “critical exponent”  $\beta \approx 0.18$ , that is also in agreement with experiment. We view this exponent not as signalling an unusual universality class, but rather as an effective power-law parametrization near a very weakly first order transition, perhaps near a mean-field tricritical point for which  $\beta = 1/4$  (up to logarithmic correction because three-dimensions is the upper critical dimension for tricritical behavior [41]). Indeed, for  $D/J_1 \lesssim 0.01$ , the transition is found to be strongly first order while it is second order and in the three-dimensional Ising universality class for  $D/J_1 \gtrsim 0.1$  [42]. We find the state above  $T_c$  to be composed of entropically favored coplanar states without long-range magnetic order and thus a Coulomb phase [3]. We hope that our study will motivate a new generation of experiments on  $\text{FeF}_3$ , perhaps even on single-crystal samples, which we would anticipate on the basis of our work to display interesting properties heretofore unexposed in highly frustrated Heisenberg pyrochlore antiferromagnets.

## Acknowledgments

We thank Bob Cava, Peter Holdsworth, Takashi Imai, Hikaru Kawamura, Seunghun Lee, Paul McClarty, Nic Shannon, Oleg Tchernyshyov and Anson Wong for useful discussions. We acknowledge Hojjat Gholizadeh for help with the pyrochlore lattice figures. This work was made possible by the facilities of the Shared Hierarchical Academic Research Computing Network (SHAR-

CNET:www.sharcnet.ca) and Compute/Calcul Canada. One of us (MG) thanks Harald Jeschke for most useful discussions regarding DFT calculations for magnetic systems. MG acknowledges support from the Canada Council for the Arts and the Perimeter Institute for Theoretical Physics. Research at PI is supported by the Government of Canada through Industry Canada and by the Province of Ontario through the Ministry of Economic Development & Innovation.

- 
- [1] J. Villain, Z. Phys. B: Condens. Matter **33**, 31 (1979).
  - [2] C. Lacroix, P. Mendels, and F. Mila, *Introduction to Frustrated Magnetism*, Springer Series in Solid-State Sciences (Springer, Heidelberg, 2011).
  - [3] C. L. Henley, Annu. Rev.: Condens. Matter Phys. **1**, 179 (2010).
  - [4] P. H. Conlon and J. T. Chalker, Phys. Rev. B **81**, 224413 (2010).
  - [5] M. J. P. Gingras and P. A. McClarty, Rep. Prog. Phys. **77**, 056501 (2014).
  - [6] M. P. Zinkin, M. J. Harris, and T. Zeiske, Phys. Rev. B **56**, 11786 (1997).
  - [7] C. Castelnovo, R. Moessner, and S. L. Sondhi, Annu. Rev.: Condens. Matter Phys. **3**, 33 (2012).
  - [8] T. Fennell, P. P. Deen, A. R. Wildes, K. Schmalzl, D. Prabhakaran, A. T. Boothroyd, R. J. Aldus, D. F. McMorrow, and S. T. Bramwell, Science **326**, 415 (2009).
  - [9] D. J. P. Morris, D. A. Tennant, S. A. Grigera, B. Klemke, C. Castelnovo, R. Moessner, C. Czternasty, M. Meissner, K. C. Rule, J.-U. Hoffmann, K. Kiefer, S. Gerischer, D. Slobinsky, R. S. Perry, Science **326**, 411 (2009).
  - [10] H. Shinaoka, Y. Motome, T. Miyake, and S. Ishibashi, Phys. Rev. B **88**, 174422 (2013).
  - [11] H. J. Silverstein, K. Fritsch, F. Flicker, A. M. Hallas, J. S. Gardner, Y. Qiu, G. Ehlers, A. T. Savici, Z. Yamani, K. A. Ross, B. D. Gaulin, M. J. P. Gingras, J. A. M. Paddison, K. Foyevtsova, R. Valenti, F. Hawthorne, C. R. Wiebe, and H. D. Zhou, Phys. Rev. B **89**, 054433 (2014).
  - [12] M. J. P. Gingras, C. V. Stager, N. P. Raju, B. D. Gaulin, and J. E. Greedan Phys. Rev. Lett. **78**, 947 (1997).
  - [13] J. S. Gardner, B. D. Gaulin, S.-H. Lee, C. Broholm, N. P. Raju, and J. E. Greedan Phys. Rev. Lett. **83**, 211 (1999).
  - [14] S.-H. Lee, C. Broholm, W. Ratcliff, G. Gasparovic, Q. Huang, T. H. Kim, and S.-W. Cheong, Nature **418**, 856 (2002).
  - [15] G. Ferey, R. De Pape, M. Leblanc, and J. Pannetier, Revue de Chimie Minérale **23**, 474 (1986).
  - [16] R. De Pape and G. Ferey, Mat. Res. Bull. **21**, 971 (1986).
  - [17] Y. Calage, M. Zemirli, J. M. Greneche, F. Varret, R. De Pape, and G. Ferey, Journal of Solid State Chemistry **69**, 197 (1987).
  - [18] J. N. Reimers, J. E. Greedan, C. V. Stager, and M. Björgvinnssen, M. A. Subramanian, Phys. Rev. B **43**, 5692 (1991).
  - [19] J. N. Reimers, J. E. Greedan, and M. Björgvinnssen, Phys. Rev. B **45**, 7295 (1992).
  - [20] A. P. Ramirez, Annu. Rev. Mater. Sci. **24**, 453 (1994).
  - [21] There are two types of third-nearest neighbors, one with two Fe-F-Fe bonds, with exchange  $J_{3a}$  and the other with three Fe-F-Fe bonds with exchange  $J_{3b}$ , in between (see Fig. 1 in the Supplemental Material [23]). In the strong coupling perturbation theory, addition of each intermediate ion increases the order of perturbation and makes the resulting super-exchange interaction smaller.
  - [22] M. Elhajal, B. Canals, R. Sunyer, and C. Lacroix, Phys. Rev. B **71**, 094420 (2005).
  - [23] See Supplementary Material at [URL], which includes additional references [1, 3–6, 29, 30].
  - [24] J. Owen and J. H. M. Thornley, Rep. Prog. Phys. **29**, 675 (1966).
  - [25] A. G. Del Maestro and M. J. P. Gingras, J. Phys.: Condens. Matter **16**, 3339 (2004); *ibid*, Phys. Rev. B **76**, 064418 (2007).
  - [26] J. B. Forsyth, P. J. Brown, and B. M. Wanklyn **21**, 2917 (1988).
  - [27] P. Perdew, K. Burke, and M. Ernzerhof, Phys. Rev. Lett. **77**, 3865 (1996).
  - [28] E. Bousquet and N. Spaldin, Phys. Rev. B **82**, 220402(R) (2010).
  - [29] T. Moriya, Phys. Rev. **120**, 91 (1960).
  - [30] N. Shannon, K. Penc, and Y. Motome, Phys. Rev. B **81**, 184409 (2010).
  - [31] <http://www.flapw.de>
  - [32] M. Cococcioni and S. de Gironcoli, Phys. Rev. B **71**, 035105 (2005).
  - [33] P. Giannozzi, S. Baroni, N. Bonini, M. Calandra, R. Car, C. Cavazzoni, D. Ceresoli, G. L. Chiarotti, M. Cococcioni, I. Dabo, A. Dal Corso, S. Fabris, G. Fratesi, S. de Gironcoli, R. Gebauer, U. Gerstmann, C. Gougousis, A. Kokalj, M. Lazzeri, L. Martin-Samos, N. Marzari, F. Mauri, R. Mazzarello, S. Paolini, A. Pasquarello, L. Paulatto, C. Sbraccia, S. Scandolo, G. Sclauzero, A. P. Seitsonen, A. Smogunov, P. Umari, R. M. Wentzcovitch, J. Phys.: Condens. Matter **21**, 395502 (2009).
  - [34] M. Enjalran and M. J. P. Gingras, Phys. Rev. B **70**, 174426 (2004).
  - [35] J. N. Reimers, A. J. Berlinsky, and A.-C. Shi, Phys. Rev. B **43**, 865 (1991).
  - [36] R. Moessner, and J. T. Chalker, Phys. Rev. Lett. **80**, 2929 (1998).
  - [37] R. Moessner and J. T. Chalker, Phys. Rev. B **58**, 12049 (1998).
  - [38] K. Binder, Journal of Computational Physics **59**, 1 (1985).
  - [39] M. S. S. Challa, D. P. Landau, and K. Binder, Phys. Rev. B **34**, 1841 (1986).
  - [40] D. P. Landau and K. Binder, *A Guide to Monte Carlo*

*Simulations in Statistical Physics* (Cambridge University Press, Cambridge, 2000)

- [41] M. J. Stephen, E. Abrahams, and J. P. Straley Phys. Rev. B **12**, 256 (1975).
- [42] We found similar behavior in a toy model with solely  $J_1 = 1$  and  $\Delta < 0$ , and so did others (P. C. W. Holdsworth, unpublished; H. Kawamura, unpublished).

## Supplemental Material

In this Supplemental Material, we present details to assist the reader with the main part of the paper. Section I provides detailed information as to how the interaction parameters of the spin Hamiltonian,  $\mathcal{H}$  in Eq. (1) in the paper, were determined from the density functional theory (DFT) calculations. Section II briefly discusses the question of quantum fluctuations of the Fe moments in  $\text{FeF}_3$  and also the dependence of the magnetic moments of the Fe and F ions on the choice of the muffin-tin radius. Section III explores how the properties of the system depend on the effective Coulomb interaction,  $U_{\text{eff}}$ . Section IV discusses the nature of the energy landscape of the bi-quadratic part of the spin Hamiltonian and how it displays a saddle point. Section V describes the orientation of the Dzyaloshinskii-Moriya (DM) vectors. Section VI shows the finite-size evolution of the energy Binder cumulant,  $U_E$ , referred to in the main text. In Section VII, we present a complementary proof to the one presented in the main text in favor of the existence coplanar states above the transition point. Section VIII discusses the details of the neutron structure function calculations reported in the main text.

### I. AB INITIO DERIVATION OF THE SPIN HAMILTONIAN FOR THE PYROCHLORE- $\text{FeF}_3$

To derive the spin Hamiltonian, we compute the energy difference between some chosen magnetic configurations using the LDA and LDA+ $U$  methods. In the following subsections, we illustrate the method for the derivation of the isotropic, i.e. Heisenberg, 4-spin ring and bi-quadratic exchanges, as well as the anisotropic terms such as the DM and the single-ion interactions.

#### A. Technical Details

To compute the Heisenberg exchange couplings, we use a super-cell containing 16 Fe and 48 F atoms (see Fig. 5), while for the 4-spin ring, bi-quadratic, single-ion and the DM coupling constants, we use the primitive cell of pyrochlore- $\text{FeF}_3$ , which contains 4 Fe atoms.

A muffin-tin radius of 2.2 (au) and 1.35 (au) is used for the Fe and F ions, respectively. The cut-off wave-vector  $k_{\text{max}} = 3.8 \text{ au}^{-1}$  is taken for the expansion of the wave function in the interstitial region and 64  $k$ -points

are picked up for performing the Brillouin zone integration. Although the magnetic moment of F is much less than Fe (see Section II), we find that choosing the direction of the fluorine magnetic moments plays a crucial role in the minimization of the total energy. Our calculations show that for a fixed direction of the Fe magnetic moments, the direction of a given fluorine moment in a Fe-F-Fe bond is uniquely determined as  $\hat{\mu}_{\text{F}} \parallel (\hat{\mu}_{\text{Fe}_1} + \hat{\mu}_{\text{Fe}_2})$ , where  $\hat{\mu}_{\text{Fe}_1}$ ,  $\hat{\mu}_{\text{Fe}_2}$  are the magnetic moment directors of the two neighboring Fe ions. As an example, choosing a direction perpendicular to the optimized direction, increases the total energy by about 14 meV per Fe ion.

### B. Spin Hamiltonian parameters

#### 1. 4-spin ring exchange

We begin with the calculation of the 4-spin ring-exchange ( $K$ ). To proceed, we compare the energy of three collinear configurations within each tetrahedron. We use  $n_i = \pm 1$  to indicate the direction of the magnetic moment of the ion at site  $i$ , along an arbitrary direction (say the  $z$ -axis). The configurations are chosen as  $C_1 \equiv \{n_1 = n_2 = n_3 = n_4 = 1\}$ ,  $C_2 \equiv \{n_1 = n_2 = 1, n_3 = n_4 = -1\}$ ,  $C_3 \equiv \{n_1 = -1, n_2 = n_3 = n_4 = 1\}$ . The total energy differences (per primitive cell) between these configurations are

$$\begin{aligned} E_1 - E_2 &= 16J_1 + 32J_2 \\ E_1 - E_3 &= 12J_1 + 24J_2 + 9K, \end{aligned} \quad (3)$$

where  $E_1$ ,  $E_2$  and  $E_3$  is the total energy of  $C_1$ ,  $C_2$  and  $C_3$  configuration, respectively. These equations yield

$$(E_1 - E_2) - \frac{4}{3}(E_1 - E_3) = -12K. \quad (4)$$

Our calculation within LDA gives  $K \sim 0.1$  meV. However, LDA+ $U$  with  $U_{\text{eff}} = 2.8$  eV gives an even smaller value for  $K$ . We therefore ignore the 4-spin ring-exchange term in the rest of our calculations.

#### 2. Heisenberg exchange parameters

The site-connectivity for the Heisenberg couplings  $J_1$ ,  $J_2$ ,  $J_{3a}$  and  $J_{3b}$  is illustrated in Fig. 4. Taking the collinear spin configurations, A, B, C and D illustrated in Fig. 5, one can show that the bi-quadratic term does not affect the energy differences, and therefore the only contributions to the total energy differences between these configurations come solely from the Heisenberg terms. Invoking the spin configurations in Fig. 5, we obtain the following expressions for the total energy (per super-cell) of each configuration:



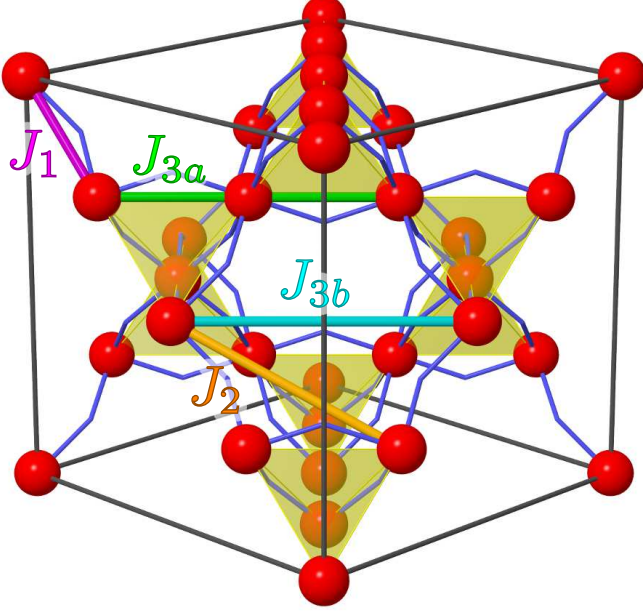


FIG. 4: The Heisenberg interactions  $J_1$ ,  $J_2$ ,  $J_{3a}$  and  $J_{3b}$  in pyrochlore  $\text{FeF}_3$ . The red spheres represent the  $\text{Fe}^{3+}$  ions. The  $\text{F}^-$  ions (not shown) are located at the bent crossings of the Fe-F-Fe (purple) bonds.

$$\begin{aligned} E_A &= 48J_1 + 96J_2 + 48J_{3,a} + 48J_{3,b} \\ E_B &= 24J_1 \\ E_C &= 48J_{3,a} + 48J_{3,b} \\ E_D &= 12J_1 - 16J_2 - 8J_{3,a} - 8J_{3,b}. \end{aligned} \quad (5)$$

LDA+ $U$  calculations with  $U_{\text{eff}} = 2.8$  eV result in the energy differences  $E_A - E_B = 866.4$  meV,  $E_A - E_C = 1627.9$  meV, and  $E_A - E_D = 1274.9$  meV, from which, assuming  $J_{3,b} \ll J_{3,a}$ , we get  $J_1 = 32.7$  meV,  $J_2 = 0.6$  meV and  $J_{3,a} = 0.5$  meV.

### 3. bi-quadratic term

To calculate the nearest-neighbor bi-quadratic coupling  $B_1$ , we seek magnetic configurations that are energetically degenerate in terms of the Heisenberg interactions, that is in the absence of spin-orbit correction. A systematic way of generating such configurations is as follows. The direction of the magnetic moments can be characterized by polar and azimuthal angles  $\theta$  and  $\phi$ , respectively. Starting from an all-in/all-out configuration, we choose two Fe ions on a tetrahedron and rotate the direction of their magnetic moment according to  $\theta'_{1,2} = \theta_{1,2} + \delta$ ,  $\phi'_{1,2} = \phi_{1,2} - 2\delta$ . For the remaining two Fe ions, we do the same but change the sign of  $\delta$ ,

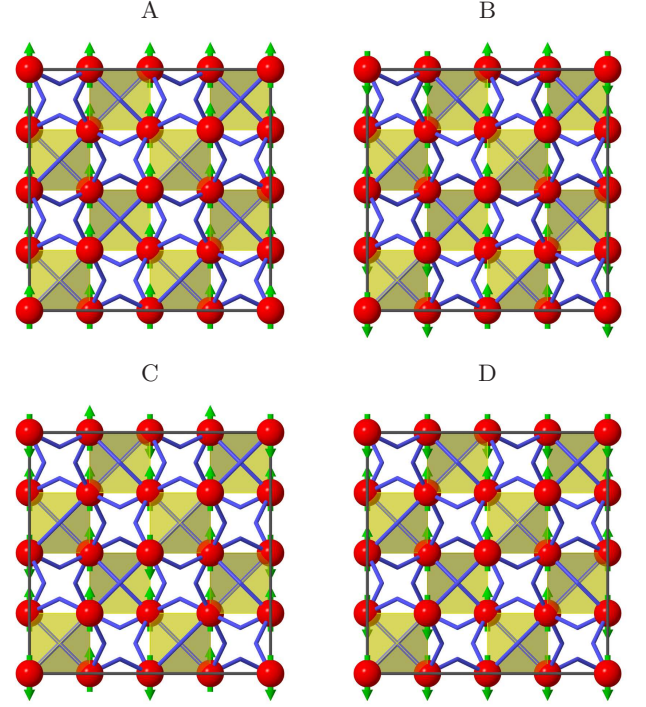


FIG. 5: The four collinear magnetic moment configurations (A, B, C and D) to derive the Heisenberg exchange interactions  $J_1$ ,  $J_2$ ,  $J_{3a}$ . The direction of magnetic moments are by the green arrows.

$\theta'_{3,4} = \theta_{3,4} - \delta$ ,  $\phi'_{3,4} = \phi_{3,4} + 2\delta$ . In this way, the vector sum of the magnetic moments remains equal to zero under this rotation. The contribution from the Heisenberg terms remaining unchanged by this rotation, the only contributions to the variation of the total energy come from the other isotropic terms within LDA and LDA+ $U$  (the anisotropic terms do not play any role because the spin-orbit coupling is not yet considered at this point). Ignoring the ring-exchange,  $K$ , and fitting the energy variations (obtained by LDA+ $U$  with  $U_{\text{eff}} = 2.8$  eV), versus  $\delta$  (shown in Fig. 6), we find the nearest-neighbor bi-quadratic coupling  $B_1 \approx 1.0$  meV.

### 4. Single-ion and Dzyaloshinskii-Moriya terms

Proceeding along, in order to derive the magnitude  $D$  of the DM interaction, we require magnetic configurations for which the full  $O(3)$  isotropic part of the Hamiltonian,  $\mathcal{H}_H + \mathcal{H}_{b.q.} + \mathcal{H}_r$ , remains unchanged.

In the absence of spin-orbit coupling (SOC), a uniform rotation of all magnetic moments does not change the total energy due to the  $O(3)$  symmetry of the non-relativistic part (see main text). However, including the spin-orbit correction to the *ab initio* calculations (LDA+ $U$ +SOC), lifts the rotational symmetry. We start from an all-in (all-out) configuration and rotate all the magnetic moments uniformly by an angle  $\phi$  around the

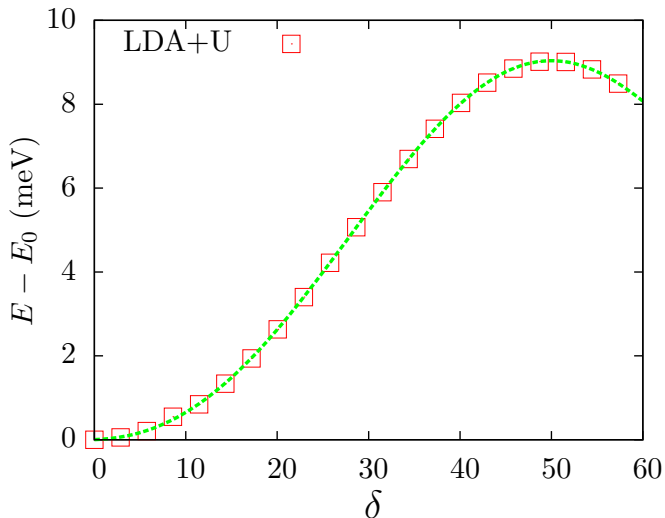


FIG. 6: Total energy difference (within LDA+ $U$ ) between all-in/all-out configuration and the configurations with the condition of zero total zero moment,  $\mathbf{S}_{\text{tot}} = 0$ , on each tetrahedron.  $\delta$  denotes the amount of rotation of spins in each configuration within a tetrahedron with respect to the all-in/all-out state ( $\theta'_{1,2} = \theta_{1,2} + \delta$ ,  $\phi'_{1,2} = \phi_{1,2} - 2\delta$ ,  $\theta'_{3,4} = \theta_{3,4} - \delta$ ,  $\phi'_{3,4} = \phi_{3,4} + 2\delta$ ). The dash line shows the fitting to the data using the bi-quadratic term of the Hamiltonian  $H_{\text{b.q.}}$ .

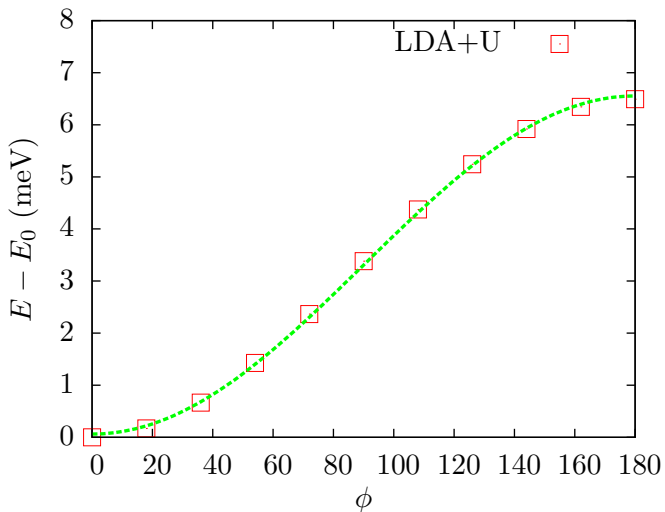


FIG. 7: Total energy difference (within LDA+ $U$ ) between the all-in/all-out configuration and the corresponding rotated one by the azimuthal angle  $\phi$ . The dash line shows the fitting to the data using the DM term in the Hamiltonian,  $H_{\text{DM}}$ .

global  $z$ -axis. Fitting the symmetry breaking relativistic corrections,  $H_{\text{DM}} + H_{\text{s.i.}}$ , to the computational total DFT energy (taking  $U_{\text{eff}} = 2.8$  eV) versus  $\phi$  (see Fig. 7), enables us to obtain  $D \approx 0.6$  meV and  $\Delta \sim 0.0$  for the DM and single-ion couplings, respectively.

## II. QUANTUM FLUCTUATIONS AND Fe & F MAGNETIC MOMENTS

Hybridization between Fe  $d$ -orbitals and F  $p$ -orbitals changes the formal ionization state of the Fe and F atoms. This covalency effect [1] results in a weak magnetic moment for F ( $\mu_{\text{F}} \approx 0.16 \mu_{\text{B}}$  within the muffin-tin sphere) along with a magnetic moment smaller than the full  $5 \mu_{\text{B}}$  ionic value for  $\text{Fe}^{3+}$  ( $\mu_{\text{Fe}} \approx 4.2 \mu_{\text{B}}$  in the muffin-tin sphere). The experimentally observed Fe long-ranged ordered moment is  $3.32(7) \mu_{\text{B}}$  [2], presumably reduced from the  $4.2 \mu_{\text{B}}$  LDA+ $U$  value by quantum fluctuations [3], which can remain sizeable for perturbatively small terms in  $\mathcal{H}$  beyond the nearest-neighbor exchange  $J_1$  [3]. The small  $0.16 \mu_{\text{B}}$  F moments would be further reduced by the quantum fluctuations of the Fe moments to which they are enslaved to.

To the best of our knowledge, the local magnetic moment ( $\sim 0.16 \mu_{\text{B}}$ ) on the F ion in  $\text{FeF}_3$  has not been measured experimentally. In part, this may be because the number of experimental studies carried out on this material has remained few until now, and it is a key purpose of our work to motivate new investigations of this compound. Perhaps Fluorine ( $^{19}\text{F}$ ) nuclear magnetic resonance (NMR) could shed light on the existence of a local moment on F (see Ref. [1]). As an example of the measurement of the magnetic moments on anion (ligand) in a transition-metal compound, we note that an oxygen (O) magnetic moment of  $0.14 \mu_{\text{B}}$  in  $\text{CuO}$  has been experimentally detected [4].

That being said, one would expect the Fe and F magnetic moments calculated within the LDA+ $U$  method to be reduced under the quantum spin fluctuations of the Fe moments not included within LDA+ $U$ . For example, the experimentally observed value (via neutron scattering [2]) of the Fe magnetic moment is  $3.32(7) \mu_{\text{B}}$  while the calculated LDA+ $U$  value is  $\sim 4.2 \mu_{\text{B}}$ . One could quite naturally ascribe such a significant reduction of 20% of the ordered moment to quantum fluctuations of the Fe magnetic moments away from the all-in/all-out ground state as we now explain.

Because of its broken global discrete symmetry nature, the all-in/all-out (AIAO) ground state stabilized by the Dzyaloshinskii-Moriya (DM) interactions would have all magnetic excitations gapped throughout the Brillouin zone and one would therefore naively expect the zero point (quantum) fluctuations to be quite small. However, because of the two completely flat zero-energy branches of magnons (zero frequency modes) associated with the original pure Heisenberg pyrochlore antiferromagnet model [3] describing this material, which then become gapped and weakly dispersive once the DM interactions are included, quantum fluctuations need not be negligible. For example, a calculation of such quantum fluctuations was carried out for the pyrochlore Heisenberg antiferromagnet with additional perturbative long-range dipolar interactions which also stabilize a broken discrete symmetry ground state [3]. A calculation of the



zero-point fluctuation-reduction of the moment in  $\text{FeF}_3$  could be carried out once an accurate experimental determination of the exchange constants and the DM interaction has been achieved (for example from an inelastic neutron scattering measurement of the spin wave dispersion below the Néel temperature). As for the F ions, the calculated magnetic moment within LDA+ $U$  is already quite small ( $\sim 0.16 \mu_B$ ) and might be difficult to detect experimentally, even more so once it is further reduced by quantum fluctuations since the F ions are tied to the Fe ions and their quantum dynamics.

In the linear augmented plane wave (LAPW) method, the computed magnetic moments depend on the choice of the radius of the muffin-tin ( $R_{\text{MT}}$ ) sphere. Here we investigate this dependency for the Fe magnetic moments, within LDA+ $U$ +SOC for the AIAO spin configuration. We show that varying  $R_{\text{MT}}$  of the Fe ions from 2.2 to 1.8 a.u., results in a slight decrease of the Fe magnetic moments from  $4.24$  to  $4.07 \mu_B$  (see Table I). Therefore, the value of  $R_{\text{MT}}$  does not have a major effect on the Fe magnetic moment in  $\text{FeF}_3$ . Hence one would still need to account for the quantum fluctuations to fill the gap between the DFT values of  $M_{\text{Fe}}$  and the experimental one. It has to be noticed that to maintain a good accuracy in the calculations, we have to enlarge the  $K_{\text{max}}$  when decreasing  $R_{\text{MT}}$ , which we have done.

TABLE I: Dependence of the Fe magnetic moment on muffin-tin radius ( $R_{\text{MT}}$ ) within LDA+ $U$ +SOC.

$R_{\text{MT}}$ (a.u.)	$M_{\text{Fe}}$ ( $\mu_B$ )
1.8	4.07
1.9	4.12
2.0	4.17
2.1	4.21
2.2	4.24

We now compare the results obtained using the generalized gradient approximation (GGA) with those obtained by LDA. For the AIAO configuration, the LDA magnetic moment of Fe is found to be  $\sim 4.03 \mu_B$ . Using GGA for the exchange-correlation functional, the magnetic moment of Fe is determined to be  $\sim 4.13 \mu_B$ . For this calculation we chose (Perdew-Burke-Ernzerhof) PBE functional [5]. Hence the usage of the GGA does not result in a significantly different Fe magnetic moment compared to LDA.

### III. DEPENDENCE OF THE RESULTS ON $U$ , $J_H$ AND $U_{\text{eff}}$

To investigate the robustness of the results presented in the main text upon changing the values of the on-site Coulomb interaction  $U$ , the Hund's exchange  $J_H$  and the effective Coulomb interaction  $U_{\text{eff}} \equiv U - J_H$ , we performed further DFT calculations by choosing different values of these parameters. First we should mention that in the DFT scheme we used,  $U$  and  $J_H$ , enters separately

in the energy functional of LDA+ $U$ . Hence, we start with the fixed value  $U_{\text{eff}} = 2.8$  eV and change the values of  $J_H$  and  $U$  accordingly. The resulting couplings of the spin Hamiltonian as well as the Fe magnetic moment within the muffin-tin sphere, for  $J_H = 0.5, 0.75, 1.0$  and  $1.25$  eV, are given in Table. II. It is evident from this table that the results are robust against the variation of  $J_H$ , provided that the effective Coulomb interaction  $U_{\text{eff}}$  remains constant. We should mention, however, that such independence of the microscopic quantities with  $U_{\text{eff}} = U - J_H$  kept constant as  $U$  and  $J_H$  are independently varied is not found in all systems. For example, consider Fig. 2 in Ref. [6] in which the magnetocrystalline anisotropy energy (MCAE) of  $\text{FeF}_2$  is computed for fixed  $U_{\text{eff}}$  while two pairs of  $U$  and  $J_H$  values are used;  $U = 6.0$  eV and  $J_H = 1.2$  eV and  $U = 5.0$  eV and  $J_H = 0.2$  eV, which both give  $U_{\text{eff}} = 4.8$  eV. The pair ( $U = 6$ ,  $J_H = 1.2$ ) gives the correct experimentally measured MCAE while the pair ( $U = 5$  and  $J_H = 0.2$ ) gives a completely different and therefore incorrect MCAE in comparison with experiment.

Next, we proceed to check the dependence of the results upon a variation of  $U_{\text{eff}}$ . For this purpose we used  $U_{\text{eff}} = 4.0$  eV (i.e.  $U = 5$  and  $J_H = 1.0$ ) and  $6.0$  eV (i.e.  $U = 7$  and  $J_H = 1.0$ ) in addition to the value  $2.8$  eV obtained by the linear response approach (see text in main paper). The computed parameters are listed in Table. III. These show that the results are quite sensitive to  $U_{\text{eff}}$ , in a sense that  $J_1$ ,  $D$  and  $B$  decrease by increasing the value of effective on-site Coulomb interaction  $U_{\text{eff}}$ . For completeness the Monte Carlo results of the Hamiltonians obtained for  $U_{\text{eff}} = 4.0$  and  $6.0$  eV are presented in Figs. 8 and 9, respectively. One sees from Figs. 8a and 9a that, as the transition temperature is decreased by increasing  $U_{\text{eff}}$ , the discontinuous nature of the transition becomes more pronounced. This is consistent with the statement made in the main text that has  $D/J_1$  is decreased, and the system approaches the isotropic Heisenberg antiferromagnet limit, the transitions become progressively more strongly first order.

The probability distributions for the AIAO order parameter  $m_n$  (Figs. 8b and 9b) and the distribution function for the four spin correlation  $R$ ,  $P(R)$  in (Figs. 8c and 9c), confirm that the general picture of coexisting AIAO and co-planar states in the vicinity of the transition point, discussed in the main body of the letter, is still operating and, therefore, does not hinge on a precise choice of  $U_{\text{eff}}$ .

### IV. ENERGY LANDSCAPE FOR A SINGLE TETRAHEDRON

In this section, we compute the classical ground state energy of the AIAO and coplanar states. We consider four classical spins residing on the corners of a single tetrahedron, interacting via a Hamiltonian  $\mathcal{H}$  that includes the antiferromagnetic Heisenberg, bi-quadratic

TABLE II: Parameters obtained from ab initio calculations (LDA+ $U$ ) with different values of  $J_H$ , and constant  $U_{\text{eff}} = 2.8$  eV.  $J_1$ ,  $J_2$  and  $J_{3a}$  are the first, second and third neighbor exchange interactions, respectively.  $B_1$  and  $D$  denote the bi-quadratic and Dzyaloshinskii-Moriya couplings, respectively.  $M_{\text{Fe}}$  is the magnetic moment of the Fe ion in the muffin-tin sphere.

$J_H$ (eV)	$U$ (eV)	$J_1$ (meV)	$J_2$ (meV)	$J_{3a}$ (meV)	$B_1$ (meV)	$D$ (meV)	$M_{\text{Fe}}$ ( $\mu_B$ )
0.5	3.30	32.484	0.590	0.541	0.967	0.567	4.244
0.75	3.55	32.607	0.591	0.541	0.961	0.570	4.244
1.00	3.80	32.731	0.592	0.540	0.954	0.573	4.243
1.25	4.05	32.861	0.592	0.541	0.948	0.576	4.243

TABLE III: Parameters of the spin Hamiltonian obtained by ab initio calculations (LDA+ $U$ ) using  $U_{\text{eff}} = 2.8, 4.0, 6.0$  eV. The last column shows the transition temperatures obtained from Monte Carlo simulations for a system size with  $N = 4 \times 6^3$

$U_{\text{eff}}$ (eV)	$J_1$ (meV)	$D/J_1$	$J_2/J_1$	$J_{3a}/J_1$	$B_1/J_1$	$T_c$ (K)
2.8	32.7	0.018	0.018	0.015	0.030	$\sim 22$
4.0	27.4	0.011	0.018	0.010	0.018	$\sim 11.5$
6.0	20.9	0.005	0.014	0.010	0.010	$\sim 4.2$

and DM interactions.

$$\mathcal{H} = \mathcal{H}_H + \mathcal{H}_{\text{b.q.}} + \mathcal{H}_{\text{DM}}. \quad (6)$$

The first term has a highly degenerate ground state manifold characterized by the two angles  $\theta$  and  $\phi$  as shown in Fig. 10. Choosing the  $z$ -axis along  $\mathbf{S}_3 + \mathbf{S}_4$  (the dashed line in Fig. 10), we can parametrize the spins within a tetrahedron by  $\theta$  and  $\phi$

$$\begin{aligned} \mathbf{S}_1 &= (-\cos \frac{\theta}{2}, 0, \sin \frac{\theta}{2}) \\ \mathbf{S}_2 &= (\cos \frac{\theta}{2}, 0, \sin \frac{\theta}{2}) \\ \mathbf{S}_3 &= (\cos \frac{\theta}{2} \cos \phi, \cos \frac{\theta}{2} \sin \phi, -\sin \frac{\theta}{2}) \\ \mathbf{S}_4 &= (-\cos \frac{\theta}{2} \cos \phi, -\cos \frac{\theta}{2} \sin \phi, -\sin \frac{\theta}{2}). \end{aligned} \quad (7)$$

The above relations enable us to write the bi-quadratic term as follows:

$$\mathcal{H}_{\text{b.q.}} = B_1 \cdot Q, \quad (8)$$

in which

$$\begin{aligned} Q &\equiv \sum_{\langle i,j \rangle} (\mathbf{S}_i \cdot \mathbf{S}_j)^2 \\ &= 1 - 2 \sin^2 \phi \cos \theta + (3 + \cos^2 \phi) \cos^2 \theta + \cos^2 \phi. \end{aligned} \quad (9)$$

The quantity  $Q$  as a function of  $\theta$  and  $\phi$ , depicted in Fig. 11, shows a minimum at  $\phi = \frac{\pi}{2}$ ,  $\theta = \cos^{-1}(1/3)$  with value  $Q = 2/3$ . This means that the ground state configuration corresponds to a non-coplanar state with an angle of  $109.47^\circ$  between each pair of spins. In this configuration, the plane of each pair is perpendicular to

the plane of the other two spins. The  $O_3$  symmetry of the bi-quadratic interaction offers the freedom to rotate this configuration by any arbitrary angle. However, it can be easily seen that the direct DM interaction selects the orientation in which the spins are aligned along the vectors connecting the corners to the center of the tetrahedron, the so called all-in/all-out (AIAO) configuration [7].

Crucially, Fig. 11 shows three saddle points for  $Q$  at  $\{\phi = 0, \theta = \frac{\pi}{2}\}$ ,  $\{\phi = \pi, \theta = \frac{\pi}{2}\}$  and  $\{\phi = \pi/2, \theta = 0\}$ . These saddle points correspond to the coplanar states discussed in the main body of the paper. There are three independent choices for constructing such a state. Depending on which two spins are considered to be collinear, the DM interaction restricts the spins to be in one of the  $xy$ ,  $xz$  or  $yz$  planes. To show this, first assume  $\mathbf{S}_1 = -\mathbf{S}_2$ ,  $\mathbf{S}_3 = -\mathbf{S}_4$  and  $\mathbf{S}_1 \perp \mathbf{S}_3$ . Then, using Eqs. (17) below, we find for the DM term

$$\begin{aligned} &\sum_{ij} \mathbf{D}_{ij} \cdot (\mathbf{S}_i \times \mathbf{S}_j) \\ &= (\mathbf{D}_{13} + \mathbf{D}_{24} - \mathbf{D}_{14} - \mathbf{D}_{23}) \cdot (\mathbf{S}_1 \times \mathbf{S}_3) \\ &= -2\sqrt{2}\hat{\mathbf{e}}_x \cdot (\mathbf{S}_1 \times \mathbf{S}_3). \end{aligned} \quad (10)$$

From this, the minimum energy condition requires that  $\mathbf{S}_1$  and  $\mathbf{S}_3$  lay in the  $yz$ -plane in such a way that their cross product gives  $\hat{\mathbf{e}}_x$ . If we choose  $\mathbf{S}_1 = -\mathbf{S}_3$ ,  $\mathbf{S}_2 = -\mathbf{S}_4$  and  $\mathbf{S}_1 \perp \mathbf{S}_2$ , we find

$$\begin{aligned} &\sum_{ij} \mathbf{D}_{ij} \cdot (\mathbf{S}_i \times \mathbf{S}_j) \\ &= (\mathbf{D}_{12} - \mathbf{D}_{14} + \mathbf{D}_{23} + \mathbf{D}_{34}) \cdot (\mathbf{S}_1 \times \mathbf{S}_2) \\ &= 2\sqrt{2}\hat{\mathbf{e}}_y \cdot (\mathbf{S}_1 \times \mathbf{S}_2). \end{aligned} \quad (11)$$

From this, we find that  $\mathbf{S}_1$  and  $\mathbf{S}_2$  lay in the  $xz$ -plane in such a way that their cross product gives  $-\hat{\mathbf{e}}_y$ . Finally,

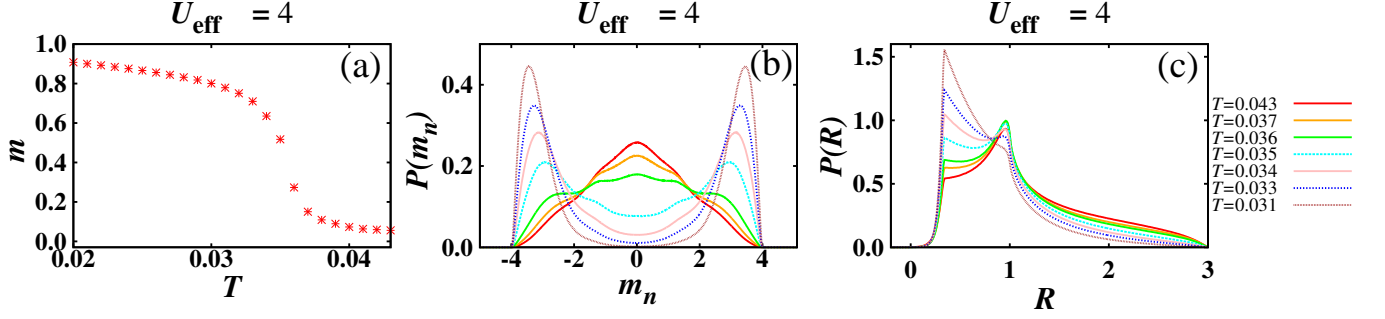


FIG. 8: (a) Variation of the AIAO order parameter,  $m$ , versus temperature  $T$  (in units of  $J_1$ ). (b) Probability distribution functions for the AIAO order parameter per tetrahedron,  $m_n$ . (c) Four spin correlation per tetrahedron,  $R$ , as defined by Eq. 20 in below, for a lattice of linear size  $L = 6$  and  $U_{\text{eff}} = 4.0$  eV.

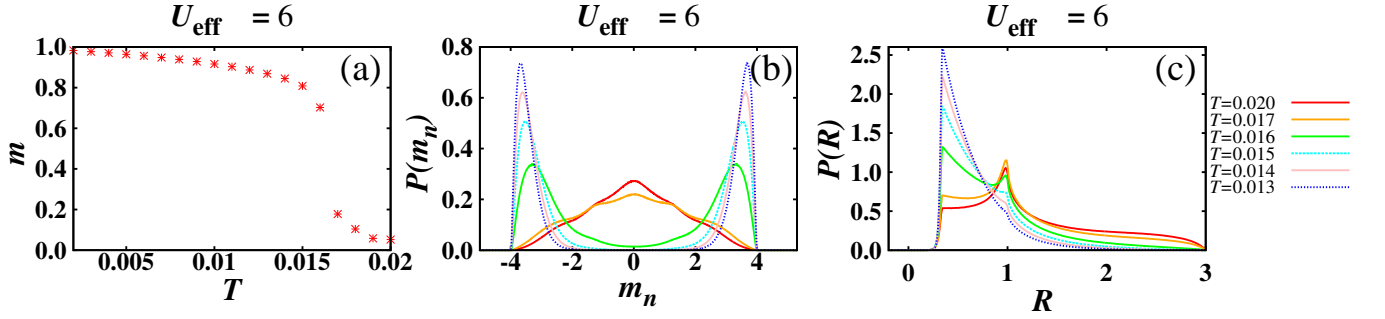


FIG. 9: (a) Variation of the AIAO order parameter,  $m$ , versus temperature  $T$  (in units of  $J_1$ ). (b) Probability distribution functions for the AIAO order parameter per tetrahedron,  $m_n$ . (c) Four spin correlation per tetrahedron,  $R$ , as defined by Eq. 20 for a lattice of linear size  $L = 6$  and  $U_{\text{eff}} = 6.0$  eV.

taking  $\mathbf{S}_1 = -\mathbf{S}_4$ ,  $\mathbf{S}_2 = -\mathbf{S}_3$  and  $\mathbf{S}_1 \perp \mathbf{S}_2$ , we get

$$\begin{aligned} & \sum_{ij} \mathbf{D}_{ij} \cdot (\mathbf{S}_i \times \mathbf{S}_j) \\ & (\mathbf{D}_{12} - \mathbf{D}_{13} + \mathbf{D}_{24} - \mathbf{D}_{34}) \cdot (\mathbf{S}_1 \times \mathbf{S}_2) \\ & 2\sqrt{2}\hat{\mathbf{e}}_z \cdot (\mathbf{S}_1 \times \mathbf{S}_2), \end{aligned} \quad (12)$$

which implies that  $\mathbf{S}_1$  and  $\mathbf{S}_2$  lay in the  $xy$ -plane in such a way that their cross product gives  $-\mathbf{e}_z$ .

The above arguments lead us to the following expressions for the energy per spin of the coplanar and all-in/all-out (AIAO) states,  $\epsilon_{\text{coplanar}}$  and  $\epsilon_{\text{AIAO}}$ , respectively, for each tetrahedron

$$\epsilon_{\text{coplanar}} = -J_1 + B_1 - D\sqrt{2} \quad (13)$$

$$\epsilon_{\text{AIAO}} = -J_1 + B_1/3 - 2D\sqrt{2}, \quad (14)$$

hence we have

$$\epsilon_{\text{coplanar}} - \epsilon_{\text{AIAO}} = \left(\frac{2B_1}{3} + D\sqrt{2}\right) > 0, \quad (15)$$

that is the ground state is AIAO for all  $B_1 > 0$  and  $D > 0$ .

## V. DZIALOSHINSKII-MORIYA (DM) VECTORS

The following minimal spin Hamiltonian,  $\mathcal{H}_{\text{min}}$ , is considered in the main part of the paper:

$$\begin{aligned} \mathcal{H}_{\text{min}} = & J_1 \sum_{\langle i,j \rangle} \sum_{a,b} \mathbf{S}_i^a \cdot \mathbf{S}_j^b \\ & + B_1 \sum_{\langle i,j \rangle} \sum_{a,b} (\mathbf{S}_i^a \cdot \mathbf{S}_j^b)^2 \\ & + D \sum_{\langle i,j \rangle} \mathbf{D}_{ab}^{ij} \cdot (\mathbf{S}_i^a \times \mathbf{S}_j^b), \end{aligned} \quad (16)$$

in which the moment  $\mathbf{S}_i$  is a classical unit vector,  $J_1 > 0$  is the nearest-neighbor antiferromagnetic exchange interaction,  $B_1 > 0$  is the nearest-neighbor bi-quadratic interaction while the last term is the anisotropic DM interaction.  $i, j = 1 \cdot N$  and  $a, b = 1, 2, 3, 4$  denote the Bravais lattice and sub-lattice indices, respectively and  $\langle i, j \rangle$  means the nearest-neighbor lattice sites. Considering a single tetrahedron, the plane which contains two

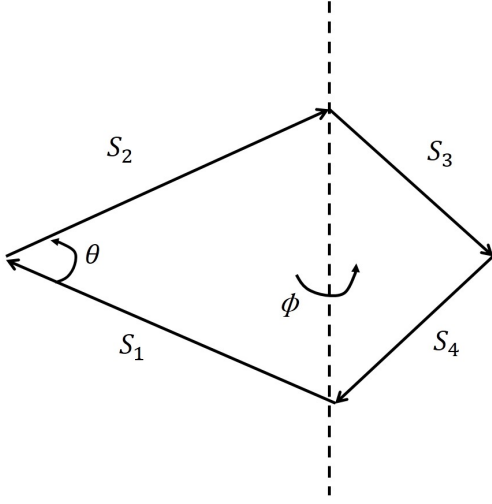


FIG. 10: A ground state configuration of four classical spins on a tetrahedron and coupled by antiferromagnetic Heisenberg interaction.

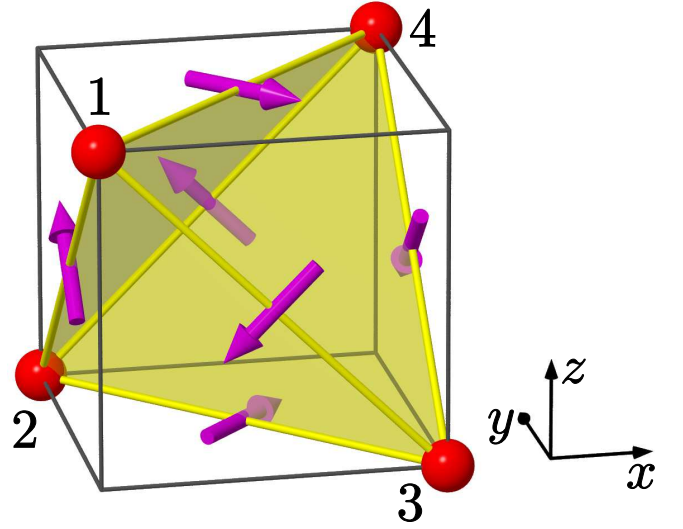


FIG. 12: Orientation of the DM vectors for a single tetrahedron.

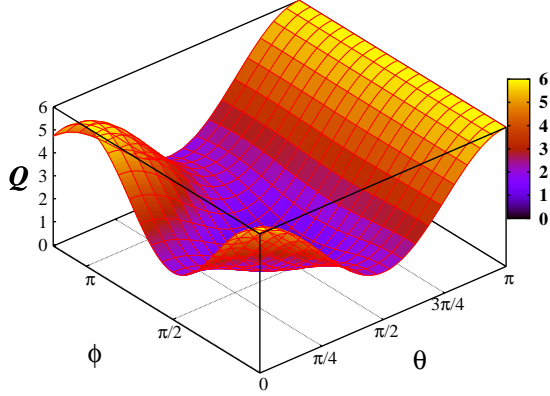


FIG. 11: Energy landscape function  $Q$  of the bi-quadratic part of  $\mathcal{H}$  alone,  $H_{b,q.} = B_1 Q(\theta, \phi)$ , in terms of  $\theta$  and  $\phi$ .

neighboring lattice points and the middle-point of the opposite bond in the tetrahedron is a mirror plane. Applying Moriya's rules [8] implies that the  $\mathbf{D}$  vector can only be perpendicular to this mirror plane or, equivalently, parallel to the opposite bond. Therefore,  $\mathbf{D}_{ab}^{ij}$ 's represent the vectors along the six directions given by:

$$\begin{aligned} \mathbf{D}_{12} &= \frac{D}{\sqrt{2}}(0, 1, 1) \\ \mathbf{D}_{13} &= \frac{D}{\sqrt{2}}(-1, 0, -1) \\ \mathbf{D}_{14} &= \frac{D}{\sqrt{2}}(1, -1, 0) \\ \mathbf{D}_{23} &= \frac{D}{\sqrt{2}}(1, 1, 0) \\ \mathbf{D}_{24} &= \frac{D}{\sqrt{2}}(-1, 0, 1) \\ \mathbf{D}_{34} &= \frac{D}{\sqrt{2}}(0, 1, -1) \end{aligned} \quad (17)$$

The orientation of the DM vectors is illustrated in Fig. 12.

There are therefore two possible values for the DM interactions between two nearest-neighbor sites and which correspond to the two directions for the  $\mathbf{D}$  vector (and keeping the same order for the cross product  $\mathbf{S}_i^a \times \mathbf{S}_j^b$ ), the “direct” DM interaction for  $D > 0$  and the “indirect” one for  $D < 0$  (Ref. [7]). For  $\text{FeF}_3$ , we find from *ab initio* DFT calculations that  $D > 0$  and that the DM interaction is therefore of the direct type.

## VI. ENERGY BINDER RATIO

The energy Binder ratio,  $U_E(T)$ , was employed in the Monte Carlo simulations to assess the order of the transition to the AIAO long-range ordered state.  $U_E(T)$  is defined as

$$U_E(T) \equiv 1 - \frac{1}{3} \frac{\langle E^4 \rangle}{\langle E^2 \rangle^2}. \quad (18)$$



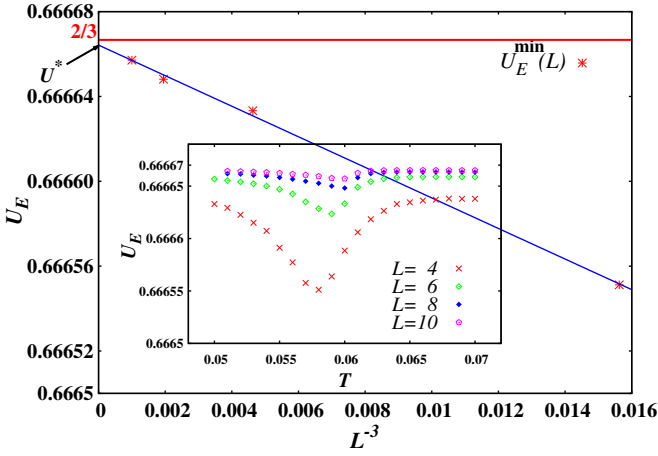


FIG. 13: Main panel: scaling of the minimum of the Binder's fourth cumulant of energy,  $U_E^{\min}(L)$  versus  $1/L^3$ . Inset: variation of  $U_E$  versus temperature,  $T$  (in units of  $J_1$ ), for lattices of linear size  $L = 4, 6, 8, 10$ .

$U_E$  tends asymptotically to  $2/3$  in both the ordered and paramagnetic phase while reaching a minimum,  $U_E^{\min}(L)$ , in the region near the transition point. For a first order transition, the finite-size scaling of  $U_E^{\min}(L)$  is given by [9]

$$U_E^{\min}(L) = U^* + AL^{-d} + \mathcal{O}(L^{-2d}), \quad (19)$$

with  $U^* < 2/3$  and where  $d = 3$  is the space dimension and  $A$  is a constant. Figure 13, which illustrates a precise linear fit of  $U_E^{\min}(L)$  versus  $L^{-3}$  with  $U^* = 0.666664(1)$ , hence very close to  $2/3$ , suggests that the transition might actually be very weakly first order [9].

## VII. VERIFICATION OF THE COPLANAR CORRELATIONS ABOVE $T_c$

In this section, we present further evidence for the existence short range coplanar correlations above  $T_c$ . In the main text we introduced a quantity  $R$ , defined as

$$R \equiv (\mathbf{S}_1 \cdot \mathbf{S}_2)(\mathbf{S}_3 \cdot \mathbf{S}_4) + (\mathbf{S}_1 \cdot \mathbf{S}_3)(\mathbf{S}_2 \cdot \mathbf{S}_4) + (\mathbf{S}_1 \cdot \mathbf{S}_4)(\mathbf{S}_2 \cdot \mathbf{S}_3), \quad (20)$$

whose probability distribution function (PDF) has a peak at  $R \approx 1$  above  $T_c$ . To assess whether this peak solely corresponds to coplanar states, we introduce another quantity,  $\tilde{R}$ , which is independent of  $R$ , and is defined within each tetrahedron as follows

$$\tilde{R} \equiv |(\mathbf{S}_1 \cdot \mathbf{S}_2)(\mathbf{S}_3 \cdot \mathbf{S}_4) - (\mathbf{S}_1 \cdot \mathbf{S}_3)(\mathbf{S}_2 \cdot \mathbf{S}_4) + (\mathbf{S}_1 \cdot \mathbf{S}_4)(\mathbf{S}_2 \cdot \mathbf{S}_3)|. \quad (21)$$

For  $T \ll J_1$ , it is highly probable that the spins within a tetrahedron are in a configuration for which  $\sum_{i=1}^4 \mathbf{S}_i \approx 0$ . We can then use the spin parametrisation in terms of the two internal (angular) degrees of freedom given

by Eq. (7). Substituting for the spins from Eq. (7) in Eqs. (20) and (21), we obtain the following two equations

$$\begin{aligned} R &= \frac{1}{2} [1 - 2 \sin^2 \phi \cos \theta + (3 + \cos^2 \phi) \cos^2 \theta + \cos^2 \phi], \\ \tilde{R} &= |1 - \sin^2 \theta (1 + \cos \phi)|. \end{aligned} \quad (22)$$

The PDF of  $\tilde{R}$  ( $P(\tilde{R})$ ) for  $L = 10$ , shown in Fig. 3c in the main text, displays a peak near  $\tilde{R} = 1$  above  $T_c$ . For an AIAO state, the values of the two above quantities are  $R = 1/3$  and  $\tilde{R} = 1/9$ . It is easy to show that the two equations  $R = 1/3$  and  $\tilde{R} = 1$  have *no common* solutions in terms of  $\theta$  and  $\phi$  and, therefore the AIAO state has no contribution causing a peak at  $\tilde{R} = 1$ . This allows us to conclude that the states giving rise to  $R = 1$  are the same as those contributing in the peak corresponding to  $\tilde{R} = 1$ . This then leaves us with the two equations ( $R = 1; \tilde{R} = 1$ ), which have the three common solutions  $\{(\phi = \pi); (\theta = \frac{\pi}{2})\}$ ,  $\{(\phi = \pi/2); (\theta = 0)\}$  and  $\{(\phi = 0); (\theta = \frac{\pi}{2})\}$ . This argument evidently proves that the states coexisting with the AIAO states above  $T_c$  are the coplanar  $xy$ ,  $xz$  and  $yz$  spin configurations discussed in Sec. IV.

## VIII. NEUTRON SCATTERING STRUCTURE FUNCTION

In this section, we calculate the neutron scattering structure function defined as

$$S(\mathbf{q}) = \sum_{i,\mu;j,\nu} \langle \mathbf{S}_{i,\mu}^\perp \cdot \mathbf{S}_{j,\nu}^\perp \rangle \exp[i\mathbf{q} \cdot (\mathbf{R}_{i,\mu} - \mathbf{R}_{j,\nu})], \quad (23)$$

where  $\mathbf{q}$  is the wave-vector transfer of the scattered neutron,  $\mathbf{S}_{i,\mu}^\perp = \mathbf{S}_{i,\mu} - \frac{(\mathbf{S}_{i,\mu} \cdot \mathbf{q})}{(\mathbf{q} \cdot \mathbf{q})} \mathbf{q}$  is the component of the spin  $\mathbf{S}_{i,\mu}$ , perpendicular to  $\mathbf{q}$  and  $\langle \dots \rangle$  denotes the thermal averaging.  $\mathbf{R}_{i,\mu} = \mathbf{T}_i + \mathbf{d}_\mu$  is the position of each of the four spins  $\mu = 1, 2, 3, 4$  in the tetrahedron unit cell  $i = 1 \dots N_{\text{cell}}$ , where  $\mathbf{T}_i$ 's are the set of primitive translation vectors of the fcc Bravais lattice.  $\mathbf{d}_\mu$  gives the position of the spins within a tetrahedron and  $N_{\text{cell}}$  denotes the total number of unit cells which is equal to  $N/4$ , with  $N$  being the total number of spins. With the geometry shown in Fig. 12 above, the vectors  $\mathbf{d}_\mu$  are given by

$$\begin{aligned} \mathbf{d}_1 &= 1/4(-1, -1, 0) \\ \mathbf{d}_2 &= 1/4(-1, 0, -1) \\ \mathbf{d}_3 &= 1/4(0, -1, -1) \\ \mathbf{d}_4 &= \mathbf{0}. \end{aligned} \quad (24)$$

Eq. 23 can be rewritten as  $S(\mathbf{q}) = \langle F(\mathbf{q})F^*(\mathbf{q}) \rangle$ , in which  $F(\mathbf{q})$  is given by

$$F(\mathbf{q}) = \sum_{i=1}^{N_{\text{cell}}} \sum_{\mu=1}^4 \left( \mathbf{S}_{i,\mu} - \frac{(\mathbf{S}_{i,\mu} \cdot \mathbf{q})}{(\mathbf{q} \cdot \mathbf{q})} \mathbf{q} \right) \exp[i\mathbf{q} \cdot (\mathbf{T}_i + \mathbf{d}_\mu)]. \quad (25)$$

In the case of long range AIAO ordering, in which all the tetrahedra have the same spin configuration, i.e

$$\begin{aligned}\mathbf{S}_1 &= \frac{1}{\sqrt{3}}(1, 1, -1) \\ \mathbf{S}_2 &= \frac{1}{\sqrt{3}}(1, -1, 1) \\ \mathbf{S}_3 &= \frac{1}{\sqrt{3}}(-1, 1, 1) \\ \mathbf{S}_4 &= \frac{1}{\sqrt{3}}(-1, -1, -1),\end{aligned}\quad (26)$$

we have  $F(\mathbf{q}) = N_{\text{cell}}f(\mathbf{q})\delta_{\mathbf{q},\mathbf{G}}$ , where  $\mathbf{G} = 2\pi(h, k, l)$  (with  $h, k, l$  being integer) denotes the fcc reciprocal lattice vectors and  $f(\mathbf{q})$  is the unit cell magnetic form factor defined as

$$f(\mathbf{q}) = \sum_{\mu=1}^4 \left( \mathbf{S}_{\mu} - \frac{(\mathbf{S}_{\mu} \cdot \mathbf{q})}{(\mathbf{q} \cdot \mathbf{q})} \mathbf{q} \right) \exp[i\mathbf{q} \cdot \mathbf{d}_{\mu}]. \quad (27)$$

Then the Bragg peaks corresponding to AIAO ordering are located at  $\mathbf{G}$ , provided the form factor at that reciprocal lattice vector does not vanish. Few examples of the Bragg peaks and values of their form factors are  $\{\mathbf{G} = 2\pi(2, 0, 2), f = 16/3\}$ ,  $\{\mathbf{G} = 2\pi(2, 2, 0), f = 16/3\}$ ,  $\{\mathbf{G} = 2\pi(2, 2, 4), f = 16/9\}$ ,  $\{\mathbf{G} = 2\pi(3, 3, \pm 1), f = 128/57\}$  and  $\{\mathbf{G} = 2\pi(1, 1, 3), f = 128/33\}$ . The reason for the vanishing of  $f(\mathbf{G})$  at some reciprocal lattice

wave-vectors, *e.g.*  $\mathbf{G} = (2, 0, 0), (1, 1, 1), (3, 3, 3)$ , is the projector  $(\mathbf{1} - \frac{\mathbf{q}\mathbf{q}}{\mathbf{q} \cdot \mathbf{q}})$  in Eq. 27 which eliminates the scattering intensity at these wave-vectors.

Fig. 14, illustrates the density plots of  $S(\mathbf{q})$  obtained from MC simulations in a lattice of linear size  $L = 10$ , for some temperatures above  $T_c$ . The thermal averaging has been done over 500 samples. This figure clearly represents the pinch-point structures of the nearest-neighbor Heisenberg pyrochlore antiferromagnet obtained by Zinkin *et al.* [11]. The location of the pinch-points for  $T = 0.1$  and  $T = 0.08$  in  $[hhl]$  plane, shown by arrows in right panel of Fig. 14, are at the wave vectors  $(1, 1, 1), (1, 1, 3), (2, 2, 0), (3, 3, 3), (2, 2, 4)$ . The pinch-points in the  $[h0l]$  plane are located at  $(2, 0, 0), (0, 0, 2), (2, 0, 4), (4, 0, 2)$ .

Close to the transition temperature, the Bragg peaks corresponding to AIAO ordering begin to grow, which as expected are located at  $(2, 0, 2), (2, 2, 0), (2, 2, 4), (1, 1, 3)$  and  $(3, 3, \pm 1)$  in Fig. 14. Some of these points, *e.g.*  $(2, 2, 0), (2, 2, 4), (1, 1, 3), (3, 3, 1)$  indicated by solid arrows in right panels of Fig. 14 correspond to the pinch-points at  $T > T_c$ , which flare up in intensity upon cooling down toward  $T_c$  and which finally form the Bragg peaks at  $T < T_c$ . This is while the other pinch-points, *i.e.*  $(1, 1, 1), (3, 3, 3)$  indicated by dashed arrows in the right panels of Fig. 14, remain as diffuse peaks upon crossing the transition. It turns out that these are reciprocal lattice vectors for which one would expect Bragg peaks if there were long range coplanar nematic order.

- 
- [1] J. Owen and J. H. M. Thornley, Rep. Prog. Phys. **29**, 675 (1966).
  - [2] G. Ferey, R. De Pape, M. Leblanc, and J. Pannetier, Revue de Chimie Minérale **23**, 474 (1986).
  - [3] A. G. Del Maestro and M. J. P. Gingras, J. Phys.: Condens. Matter **16**, 3339 (2004); *ibid*, Phys. Rev. B **76**, 064418 (2007).
  - [4] J. B. Forsyth, P. J. Brown, and B. M. Wanklyn **21**, 2917 (1988).
  - [5] P. Perdew, K. Burke, and M. Ernzerhof, Phys. Rev. Lett. **77**, 3865 (1996).
  - [6] E. Bousquet and N. Spaldin, Phys. Rev. B **82**, 220402(R) (2010).
  - [7] M. Elhajal, B. Canals, R. Sunyer, and C. Lacroix, Phys. Rev. B **71**, 094420 (2005).
  - [8] T. Moriya, Phys. Rev. **120**, 91 (1960).
  - [9] D. P. Landau and K. Binder, *A Guide to Monte Carlo Simulations in Statistical Physics* (Cambridge University Press, Cambridge, 2000).
  - [10] N. Shannon, K. Penc, and Y. Motome, Phys. Rev. B **81**, 184409 (2010).
  - [11] M. P. Zinkin, M. J. Harris, and T. Zeiske, Phys. Rev. B **56**, 11786 (1997).

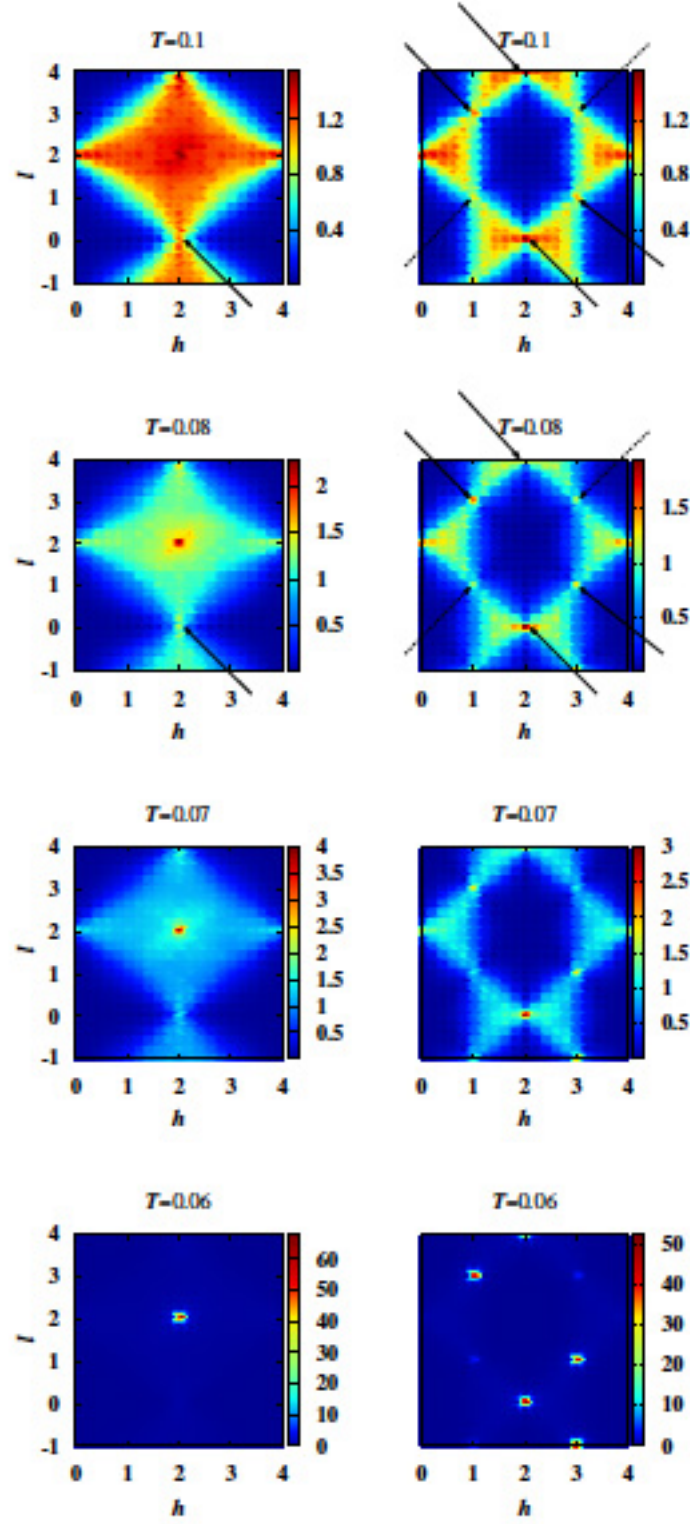


FIG. 14: Density plot of neutron structure function  $S(\mathbf{q})$  obtained by Monte Carlo simulations on the pyrochlore lattice of linear size  $L = 10$  in the (Left column)  $[h0l]$  and (Right column)  $[hhl]$  planes at the temperatures  $T/J_1 = 0.1, 0.08, 0.07, 0.06$ . Note that the intensity scale (right color bar) evolves as  $T$  approaches  $T_c$ . The arrows in the top panels, display the location of the pinch-points at  $T = 0.1, 0.08$